

Nanoscale Manipulation of Wrinkle-Pinned Vortices in Iron-Based Superconductors

Peng Fan,[#] Hui Chen,[#] Xingtai Zhou,[#] Lu Cao, Geng Li, Meng Li, Guojian Qian, Yuqing Xing, Chengmin Shen, Xiancheng Wang, Changqing Jin, Genda Gu, Hong Ding, and Hong-Jun Gao*



Cite This: <https://doi.org/10.1021/acs.nanolett.3c00982>



Read Online

ACCESS |

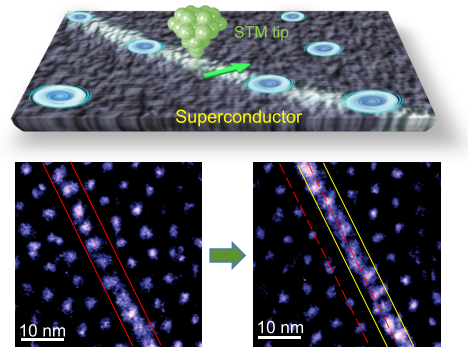
Metrics & More

Article Recommendations

Supporting Information

ABSTRACT: The controlled manipulation of Abrikosov vortices is essential for both fundamental science and logical applications. However, achieving nanoscale manipulation of vortices while simultaneously measuring the local density of states within them remains challenging. Here, we demonstrate the manipulation of Abrikosov vortices by moving the pinning center, namely one-dimensional wrinkles, on the terminal layers of Fe(Te,Se) and LiFeAs, by utilizing low-temperature scanning tunneling microscopy/spectroscopy (STM/S). The wrinkles trap the Abrikosov vortices induced by the external magnetic field. In some of the wrinkle-pinned vortices, robust zero-bias conductance peaks are observed. We tailor the wrinkle into short pieces and manipulate the wrinkles by using an STM tip. Strikingly, we demonstrate that the pinned vortices move together with these wrinkles even at high magnetic field up to 6 T. Our results provide a universal and effective routine for manipulating wrinkle-pinned vortices and simultaneously measuring the local density of states on the iron-based superconductor surfaces.

KEYWORDS: Abrikosov vortex, manipulation, scanning tunnelling microscopy, iron-based superconductors, nanowrinkle



The manipulation of vortices, which host a quantized magnetic flux in a type-II superconductor, is a crucial step toward developing applications in topological quantum computation. The normal-state vortex core has a radius of the scale of superconducting coherence length ξ . Around the vortex core, the circulating supercurrent has a decay length of magnetic penetration depth λ .¹ The vortices tend to be pinned at the defected sites where superconducting is suppressed. Vortices can perform clock logic operations by forming a ratchet mechanism² or control spin in an adjacent diluted magnetic semiconductor.³ In recent years, it has been demonstrated by scanning tunnelling microscopy (STM) that vortices in iron-based superconductors (IBSs) host Majorana zero mode (MZM),^{4–12} which has potential applications in topological quantum computation.^{13,14} Manipulating and braiding MZMs are fundamental operations in topological quantum computation. The complete process of braiding MZMs needs to be achieved in a topological region, which is normally tens to a hundred nanometers in $\text{FeTe}_{0.55}\text{Se}_{0.45}$.⁹ Meanwhile, the operation of braiding MZMs itself requires precision. Therefore, nanoscale manipulation of vortices is crucial but still lacks in IBSs.

Several different methods have been applied to manipulate individual Abrikosov vortices in superconductors. By using magnetic force microscopy (MFM)^{15,16} and scanning superconducting quantum interference device (SQUID) microscopy,^{17–19} the vortices are driven by the magnetic force or

local mechanical stress. However, these methods have limited spatial precision, with MFM having a precision range of 10–100 nm and SQUID having a range of 100 nm.²⁰ In the superconducting film, the vortices are driven by laser beam-induced²¹ and tunneling current-induced²² heating effects, which create a micron-sized hotspot. Control of individual Abrikosov vortices by all the methods mentioned above, where the driving forces have a large influence on size, requires vortices with large sizes and a long distance between vortices. Meanwhile, the pinning potential competes with repulsive interaction between vortices. The final location of vortex depends on the balance of this competition and is limited by the pinning centers. In IBSs, the small distance (tens of nanometers) between vortices at high magnetic field on the order of Tesla results in a stronger repulsive force between vortices, which makes it even more difficult to control the vortices. In addition, none of the methods above are capable of both manipulating the vortex and measuring the local density of the states (LDOS) within the vortex simultaneously. Therefore, achieving nanoscale manipulation of vortices with

Received: March 14, 2023

Revised: May 5, 2023

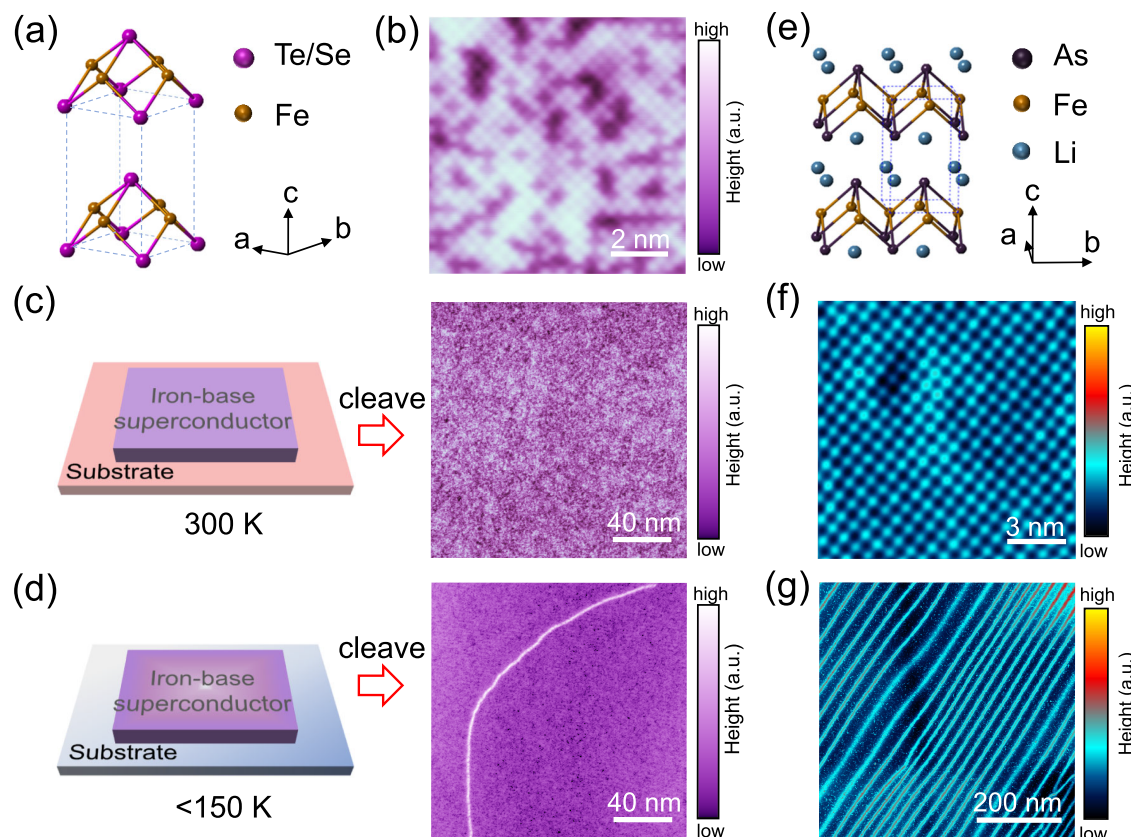


Figure 1. 1D wrinkles on FeTe_{0.55}Se_{0.45} and LiFeAs. (a) Atomic structure of FeTe_{0.55}Se_{0.45}. (b) Atomically resolution STM image ($V_s = -10$ mV, $I_t = 100$ pA) of FeTe_{0.55}Se_{0.45}. (c) Schematic of cleaving process at 300 K and STM image ($V_s = -10$ mV, $I_t = 10$ pA) of clean surface. (d) Schematic of cleaving process at 150 K and STM image ($V_s = -10$ mV, $I_t = 10$ pA) of the cleaved surface. The bright stripe is a 1D wrinkle. (e) Atomic structure of LiFeAs. (f) Atomically resolution STM image ($V_s = -5$ mV, $I_t = 100$ pA) of LiFeAs. (g) The STM image ($V_s = -30$ mV, $I_t = 30$ pA) of LiFeAs shows wrinkles on the surface (the electron temperature of STM#1: $T_{\text{eff}} \#1 \approx 752$ mK, the electron temperature of STM#2: $T_{\text{eff}} \#2 \approx 715$ mK).

a controllable final location and simultaneous measurement of the LDOS within the vortex of bulk IBSs remains challenging.

In this work, by employing STM, we achieve the manipulation and detection of the local density of states of the vortices which are pinned by the nanoscale wrinkles on the surface of some IBSs, namely FeTe_{0.55}Se_{0.45} and LiFeAs. The wrinkles which are controllably created through a low-temperature cleaving process trap one-dimensional vortex lattice due to the suppression of superconductivity on some of the wrinkles. In some wrinkle-pinned vortices, we observe sharp ZBPs, which never split or shift when moving away from the vortex core. The wrinkles are tailored and moved at the nanoscale by the STM tip. As a result, the pinned vortices are driven together with wrinkles. Despite the strong repulsive force between vortices under an external magnetic field perpendicular to the sample surface of 6 T, the vortices move simultaneously with the pinning center, i.e., the wrinkles. This vortex-control technique opens up a new avenue for manipulating exotic vortex bound states and studying vortex entanglement²³ in IBSs, moreover, as well as other layered superconductors.

We first study the controllable construction of wrinkles on two typical IBSs, FeTe_{0.55}Se_{0.45} and LiFeAs (Figures 1). The wrinkles, which are one-dimensional (1D) corrugated structures commonly observed in graphene,^{24–29} transition metal disulfide,^{30–36} and other layered materials,³⁷ are typically introduced by prestraining substrate²⁷ or synthesizing the

material with a different thermal expansion coefficient than the substrate.³⁸ Here, we intentionally cool down the cleave temperature to introduce wrinkles at the as-cleaved surfaces of the FeTe_{0.55}Se_{0.45} single crystal, whose atomic structure and atomically resolved STM image are shown in Figure 1a and Figure 1b, respectively. We perform the crystal cleavage at both room temperature and low temperature (150 K), respectively. As a result, the STM image shows a flat as-cleaved surface without corrugations at a cleaving temperature of 300 K (Figure 1c). In contrast, the wrinkles appearing as one-dimensional ridges are more frequently observed at a cleaving temperature lower than 150 K (Figure 1d), indicating that the wrinkles are generated during cleavage. We attribute the stability of the wrinkles at low temperature to the non-dissipative of stress during the cleaving process. Similarly, we detect wrinkles on the lithium-terminated surface of LiFeAs (Figures 1e–f) and find that they are more likely to appear under low cleaving temperatures. The wrinkles appeared as bright stripes arranged in arrays on the surface of LiFeAs (Figure 1g).

We next study the pinning effects at the wrinkle regions. The pinning centers, such as atomic vacancies,³⁹ nanostrain,⁴⁰ and crystal disruption,⁴¹ can trap magnetic flux due to the suppression of Cooper pairs. Here, we demonstrate that some of the wrinkles of FeTe_{0.55}Se_{0.45} and LiFeAs can trap vortices. To investigate the influence of wrinkles on the superconducting parameter, we detected the spectra across the

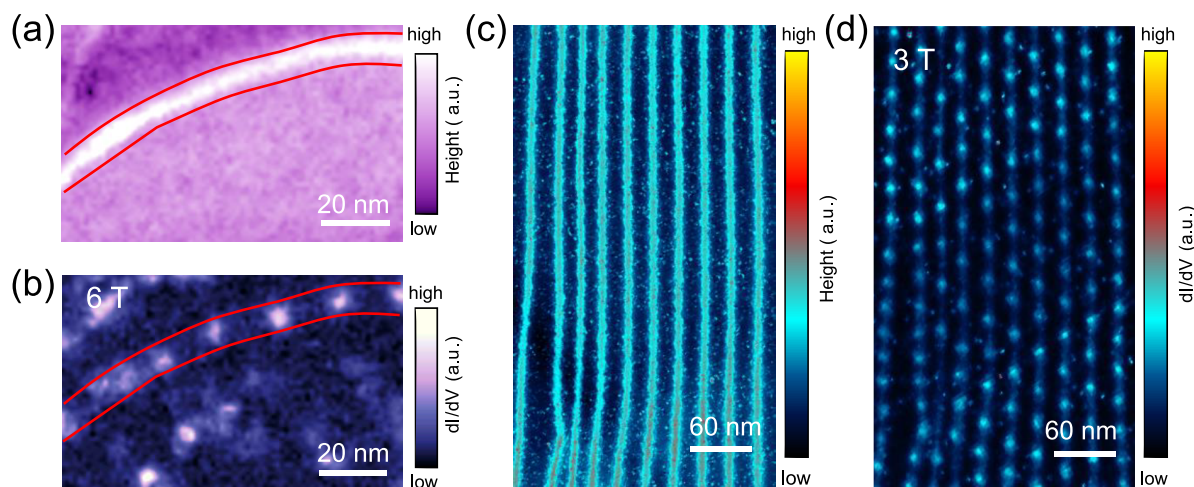


Figure 2. 1D vortex lattice pinned on wrinkles. (a) STM image ($V_s = -10$ mV, $I_t = 10$ pA) of a wrinkle on $\text{FeTe}_{0.55}\text{Se}_{0.45}$. (b) Zero-bias-conductance (ZBC) map ($V_s = -10$ mV, $I_t = 100$ pA) detected in the area of (a) with an extra magnetic field of 6 T. The vortices with a distance of about 18 nm between each other are pinned on the wrinkle, indicated by red lines. (c) STM image ($V_s = -30$ mV, $I_t = 30$ pA) of wrinkles on LiFeAs. (d) ZBC map ($V_s = -5$ mV, $I_t = 200$ pA) detected in the area of (c) with an extra magnetic field of 3 T. The vortices are pinned on the array of wrinkles ($T_{\text{eff}}\#1 \approx 752$ mK, $T_{\text{eff}}\#2 \approx 715$ mK).

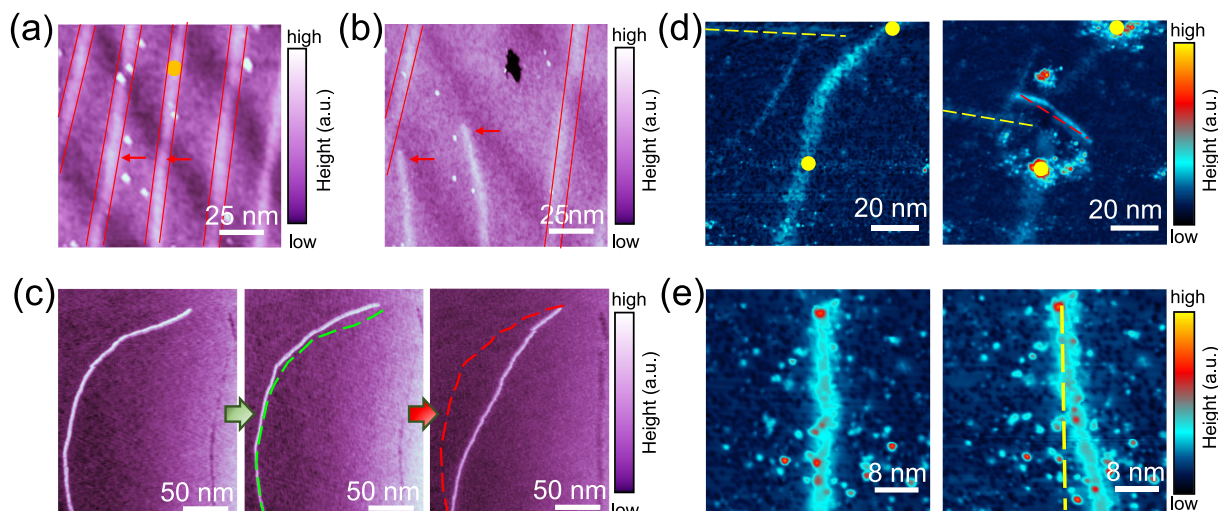


Figure 3. Controllable tailoring and moving of wrinkles. (a) STM image of $\text{FeTe}_{0.55}\text{Se}_{0.45}$ ($V_s = -10$ mV, $I_t = 10$ pA) with several wrinkles in it. Wrinkles are highlighted by red lines. The bright dots are clusters on the surface of $\text{FeTe}_{0.55}\text{Se}_{0.45}$. (b) STM image ($V_s = -10$ mV, $I_t = 10$ pA) of the same area in (a). We approach the tip and dig a hole on the surface. The two wrinkles (pointed by red arrows in a and b) breaks up because of the tensile strain. The undisturbed wrinkles are highlighted by red lines. (c) A series of STM images ($V_s = -10$ mV, $I_t = 10$ pA) show a sequence of right-sliding and left-sliding of a wrinkle on $\text{FeTe}_{0.55}\text{Se}_{0.45}$. (d) STM images ($V_s = -30$ mV, $I_t = 30$ pA) show tailoring wrinkles by using STM tip on LiFeAs. The yellow balls indicate the location where we pulse the tip. (e) STM images ($V_s = -30$ mV, $I_t = 30$ pA) show sliding of a wrinkle on LiFeAs ($T_{\text{eff}}\#1 \approx 752$ mK, $T_{\text{eff}}\#2 \approx 715$ mK).

wrinkles in $\text{FeTe}_{0.55}\text{Se}_{0.45}$ and LiFeAs, respectively. In $\text{FeTe}_{0.55}\text{Se}_{0.45}$, the spectra detected beyond the wrinkle show hard superconducting gaps (Figure S1a–b), while the superconducting gap becomes small and soft upon entering the wrinkle. In LiFeAs, the superconducting gaps on the wrinkle show a suppression of coherence peaks (Figure S1c–d), which are in accordance with the results of type-II wrinkles in LiFeAs reported in a previous work.³⁷ We attribute the suppression of Cooper pairs to the local strain around wrinkles.

To demonstrate the pinning effect of the wrinkles, we carry out the zero-bias conductance (ZBC) maps and display them on Figure 2. We acquire the corresponding ZBC map at 6 T in the surface region of $\text{FeTe}_{0.55}\text{Se}_{0.45}$ with wrinkles (Figure 2a–b). Vortices are pinned along the wrinkles and form one-dimensional (1D) vortex chains. We observed similar results in

the type-II wrinkle regions of LiFeAs³⁷ where the vortices are highly ordered along the wrinkles and form a 1D vortex chain at 3 T (Figure 2c–d). The distance between vortices trapped within one wrinkle is roughly uniform in both $\text{FeTe}_{0.55}\text{Se}_{0.45}$ and LiFeAs, indicating that the pinning force in the wrinkles is homogeneous.

We also detected the dI/dV spectra across the wrinkle-pinned vortex. Intriguingly, despite the stress in the wrinkle, we observe a zero-bias peak (ZBP) in the core of some wrinkle-pinned vortices in both $\text{FeTe}_{0.55}\text{Se}_{0.45}$ (Figure S2a–c) and LiFeAs (Figures S2d–f). From the intensity plot of a series of spectra detected in the wrinkle-pinned vortex on $\text{FeTe}_{0.55}\text{Se}_{0.45}$ (Figures S2c) and LiFeAs (Figure S2f), the ZBPs never split or shift at positions away from the vortex center. The behaviors of ZBPs are the same as those in previous work on

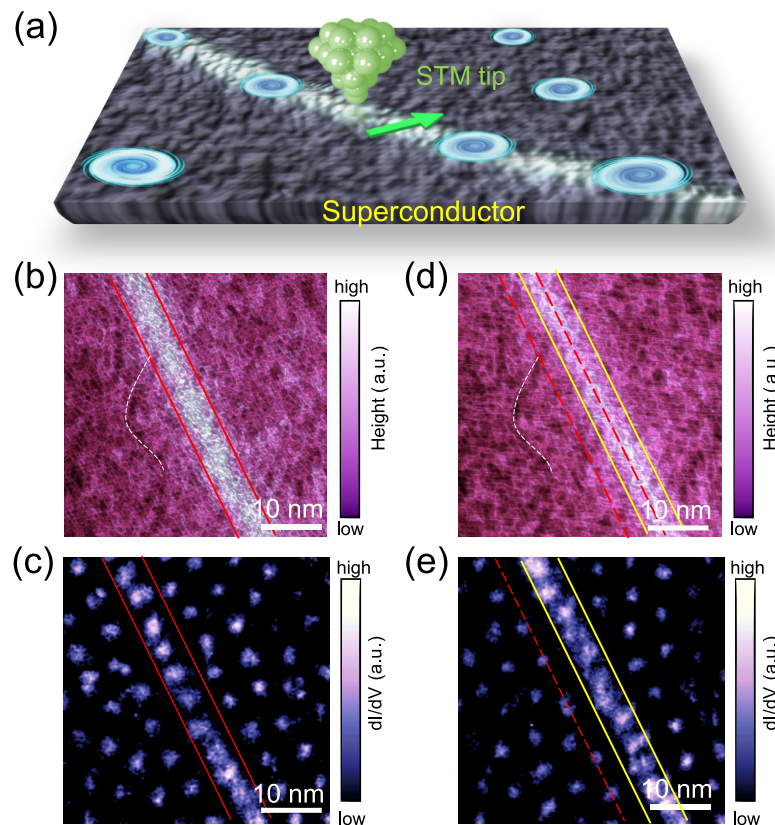


Figure 4. Control of vortex motion by manipulating wrinkles. (a) Schematic of the movement of wrinkle-pinned vortex by using STM tip. (b and c) STM image (b) ($V_s = -10$ mV, $I_t = 100$ pA) and zero-bias dI/dV mapping (c) ($V_s = -10$ mV, $I_t = 100$ pA) showing a wrinkle and as-pinned vortices at a magnetic field of $B_z = 6$ T. (d and e) STM image (d) ($V_s = -10$ mV, $I_t = 100$ pA) and zero-bias dI/dV mapping (e) ($V_s = -10$ mV, $I_t = 100$ pA) showing the wrinkle and as-pinned vortices after manipulation, indicating the controlled sliding of wrinkle and corresponding 1D pinned vortices ($T_{\text{eff}} \#1 \approx 752$ mK, $T_{\text{eff}} \#2 \approx 715$ mK).

$\text{FeTe}_{0.55}\text{Se}_{0.45}$ ^{4,9,11} where the ZBPs are attributed to MZMs. In addition, MZMs are reported to exist in impurity-assisted vortices⁷ and Abrikosov vortices in biaxial charge density wave (CDW) regions⁸ in LiFeAs. Here, the ZBPs in wrinkle-pinned vortices on $\text{FeTe}_{0.55}\text{Se}_{0.45}$ and LiFeAs are possibly MZMs. However, due to the electron temperatures in our work being ~ 752 mK for STM#1 and ~ 715 mK for STM#2 (Figure S3), we cannot distinguish the ZBP from the low-lying Caroli-de Gennes-Matricone (CdGM) state. Further experiments at very low temperatures (~ 100 mK electron temperature)¹¹ are needed.

After investigating the pinning effects of the wrinkle, we achieve the manipulation of wrinkles in $\text{FeTe}_{0.55}\text{Se}_{0.45}$ and LiFeAs. First, we tailor the wrinkle in $\text{FeTe}_{0.55}\text{Se}_{0.45}$ by approaching the tip toward the surface (orange ball in Figure 3a) and controlled crashing the tip on the surface, which results in a vacancy nanoisland (black hollow in Figure 3b). The controlled crash modifies the local strain field around the wrinkles, causing two of the wrinkles (pointed by red arrows) to break up and move away, while the other two wrinkles on the sides remain unchanged. Subsequently, we move the wrinkle at the atomic scale, as demonstrated by the series of STM images in Figure 3c, which show the sliding of a wrinkle on $\text{FeTe}_{0.55}\text{Se}_{0.45}$. We achieve the movement of wrinkle by approaching the tip close to the surface and scanning across the wrinkle (details see Method). As a result, the wrinkle is dragged by the tip and slides with a distance ranging from several to tens of nanometers, allowing for the movement of

wrinkles along different directions without causing damage or structure defects.

In addition to the $\text{FeTe}_{0.55}\text{Se}_{0.45}$, we have demonstrated that these manipulating processes, including tailoring and moving the wrinkle, can extend to the surface of LiFeAs (Figures 3d–e). After being tailored at two positions by an STM tip, the wrinkle is cut into a short piece (Figure 3d), allowing for the artificial fabrication of short wrinkles that can trap vortices with a desired number. The wrinkle in LiFeAs is also moved by scanning across the wrinkle with a short tip–sample distance, as shown in Figure 3e. The successful application of manipulation methods to wrinkles in $\text{FeTe}_{0.55}\text{Se}_{0.45}$ and LiFeAs proves that it is a universal technique, which could potentially be utilized in other IBSs.

The controllable tailoring and moving of wrinkles immediately open an opportunity to manipulate the vortices trapped by them, as shown in the schematic (Figure 4a). We have achieved the manipulation of vortices around 1D wrinkles at the surface of $\text{FeTe}_{0.55}\text{Se}_{0.45}$. The original topographic image with a wrinkle and the corresponding ZBC map of the same area detected at 6 T are displayed in Figure 4b and Figure 4c, respectively. In the ZBC map, vortices are trapped in the wrinkle and form an ordered vortex chain. Then the wrinkle is pushed forward about 5 nm (Figure 4d–e), with the original location marked by dashed red lines in the topography (Figure 4d) and the corresponding ZBC map (Figure 4e) for comparison. Owing to the strong pinning force of the wrinkle, the pinned vortex chain moves together with the wrinkle and

stays stable at the final location, whereas normally in a sample without pinning centers, the vortices relax into a triangular vortex lattice after removing the external force at such high magnetic fields, due to the strong repulsive interaction between vortices.²² Meanwhile, the vortices outside the wrinkle rearrange due to the strong repulsive force between vortices. Throughout the entire process, including manipulating the wrinkle and detecting the ZBC map, the magnetic field is kept constant at 6 T.

In summary, we intentionally introduce nanowrinkles on both $\text{FeTe}_{0.55}\text{Se}_{0.45}$ and LiFeAs through low-temperature cleavage. The wrinkles trap a one-dimensional vortex chain, due to the suppression of Cooper pairs by a local strain. In some wrinkle-pinned vortices, robust ZBPs are observed, which are possibly MZMs. By employing an STM tip, we tailor a long wrinkle into short pieces and precisely move them. The vortices move together with the wrinkle due to the pinning effect, which provides a way to manipulate vortices. The generation and manipulation of vortex-pinning wrinkles, and simultaneous detection of LDOS within vortices, open up new opportunities for studying the interaction of bound states in adjacent vortices on layered superconductors and may lead to new applications in quantum technologies.

■ EXPERIMENTAL METHOD

Single Crystal Growth. High-quality single crystals of $\text{FeTe}_{0.55}\text{Se}_{0.45}$ ⁴ and LiFeAs⁴² are grown using the self-flux method. The $\text{FeTe}_{0.55}\text{Se}_{0.45}$ crystal and LiFeAs crystal are mounted on an STM sample holder in a glovebox and transferred to an ultrahigh-vacuum chamber.

Scanning Tunneling Microscopy/Spectroscopy. The samples are cleaved *in situ* and immediately transferred into an STM scanner. The STM experiments on $\text{FeTe}_{0.55}\text{Se}_{0.45}$ are carried out in an ultrahigh vacuum (1×10^{-11} mbar) LT-STM system (USM-1300s-³He, STM1#), which can apply a perpendicular magnetic field up to 11 T. The STM experiments on LiFeAs are carried out in an ultralow-temperature STM system (USM-1300s-³He, STM2#) equipped with 9–2–2 T vectorial magnets. STM images are acquired in the constant-current mode with a tungsten tip. The voltage offset calibration is followed by a standard method of overlapping points of I – V curves. Differential conductance (dI/dV) spectra are acquired by a standard lock-in amplifier at a frequency of 973.1 Hz, under modulation voltage $V_{mod} = 0.1$ mV. A low temperature of 0.4 K is achieved by a single-shot ³He cryostat.

Manipulation of Wrinkles. In the tip crashing process, the feedback is off. The tip is approached 1 nm closer toward the sample surface within a very short time (50 ms), which induces the tip crash on the sample surface. Afterward, the sample bias is changed into 1 V and kept for 1 s. Finally, the tip is withdrawn from the sample surface with the feedback on within a very short time (50 ms). In the tip-induced moving process, the feedback is on. The scanning parameter is set to be $I_{sep\text{point}} = 5$ nA, $V_{sample} = -1$ mV, which positions the tip closer to the sample surface. Then the tip moves across the wrinkle, which results in the displacement of the wrinkle along the same direction with the tip.

■ ASSOCIATED CONTENT

SI Supporting Information

The Supporting Information is available free of charge at <https://pubs.acs.org/doi/10.1021/acs.nanolett.3c00982>.

The characterization of the superconductivity across wrinkles on $\text{FeTe}_{0.55}\text{Se}_{0.45}$ and LiFeAs; Zero bias peaks in the wrinkle-pinned vortices; Calibration of electronic temperature. (PDF)

■ AUTHOR INFORMATION

Corresponding Author

Hong-Jun Gao – Beijing National Center for Condensed Matter Physics and Institute of Physics and School of Physical Sciences, Chinese Academy of Sciences, Beijing 100190, P. R. China; Hefei National Laboratory, Hefei, Anhui 230088, P. R. China;  orcid.org/0000-0002-6766-0623; Email: hjgao@iphy.ac.cn

Authors

Peng Fan – Beijing National Center for Condensed Matter Physics and Institute of Physics and School of Physical Sciences, Chinese Academy of Sciences, Beijing 100190, P. R. China

Hui Chen – Beijing National Center for Condensed Matter Physics and Institute of Physics and School of Physical Sciences, Chinese Academy of Sciences, Beijing 100190, P. R. China; Hefei National Laboratory, Hefei, Anhui 230088, P. R. China;  orcid.org/0000-0002-3369-8113

Xingtai Zhou – Beijing National Center for Condensed Matter Physics and Institute of Physics and School of Physical Sciences, Chinese Academy of Sciences, Beijing 100190, P. R. China;  orcid.org/0000-0002-2455-8303

Lu Cao – Beijing National Center for Condensed Matter Physics and Institute of Physics and School of Physical Sciences, Chinese Academy of Sciences, Beijing 100190, P. R. China

Geng Li – Beijing National Center for Condensed Matter Physics and Institute of Physics and School of Physical Sciences, Chinese Academy of Sciences, Beijing 100190, P. R. China; Hefei National Laboratory, Hefei, Anhui 230088, P. R. China;  orcid.org/0000-0002-3347-7222

Meng Li – Beijing National Center for Condensed Matter Physics and Institute of Physics and School of Physical Sciences, Chinese Academy of Sciences, Beijing 100190, P. R. China

Guojian Qian – Beijing National Center for Condensed Matter Physics and Institute of Physics and School of Physical Sciences, Chinese Academy of Sciences, Beijing 100190, P. R. China

Yuqing Xing – Beijing National Center for Condensed Matter Physics and Institute of Physics and School of Physical Sciences, Chinese Academy of Sciences, Beijing 100190, P. R. China

Chengmin Shen – Beijing National Center for Condensed Matter Physics and Institute of Physics and School of Physical Sciences, Chinese Academy of Sciences, Beijing 100190, P. R. China

Xiancheng Wang – Beijing National Center for Condensed Matter Physics and Institute of Physics and School of Physical Sciences, Chinese Academy of Sciences, Beijing 100190, P. R. China;  orcid.org/0000-0001-6263-4963

Changqing Jin — *Beijing National Center for Condensed Matter Physics and Institute of Physics and School of Physical Sciences, Chinese Academy of Sciences, Beijing 100190, P. R. China*
Genda Gu — *Condensed Matter Physics and Materials Science Department, Brookhaven National Laboratory, Upton, New York 11973, United States*
Hong Ding — *Beijing National Center for Condensed Matter Physics and Institute of Physics, Chinese Academy of Sciences, Beijing 100190, P. R. China*

Complete contact information is available at:
<https://pubs.acs.org/10.1021/acs.nanolett.3c00982>

Author Contributions

#P.F., H.C., and X.Z. contributed equally to this work. H.-J.G. conceived and supervised the project. P.F., H.C., L.C., X.Z., and M.L. performed STM experiments. G.G. provided FeTe_{0.55}Se_{0.45} single crystal. X.W. and C.J. prepared LiFeAs single crystal. P.F., H.C., G.L., and H.-J.G. processed experimental data and wrote the manuscript with input from all other authors. All the authors participated in analyzing experimental data, plotting figures, and writing the manuscript.

Notes

The authors declare no competing financial interest.

ACKNOWLEDGMENTS

The work is supported by grants from the National Natural Science Foundation of China (61888102, 52022105), the National Key Research and Development Projects of China (2018YFA0305800 and 2019YFA0308500), and the Chinese Academy of Sciences (XDB28000000, XDB30000000), the CAS Project for Young Scientists in Basic Research (YSBR-003) and the Key Research Program of Chinese Academy of Sciences (ZDBS-SSW-WHC001), the Innovation Program of Quantum Science and Technology (2021ZD0302700). The work at BNL is supported by grants from US DOE, Basic Energy Sciences (DE-SC0012704, DE-FG02-99ER45747).

REFERENCES

- (1) Blatter, G.; Feigel'man, M. V.; Geshkenbein, V. B.; Larkin, A. I.; Vinokur, V. M. Vortices in high-temperature superconductors. *Rev. Mod. Phys.* **1994**, *66* (4), 1125–1388.
- (2) Hastings, M. B.; Reichhardt, C. J.; Reichhardt, C. Ratchet cellular automata. *Phys. Rev. Lett.* **2003**, *90* (24), 247004.
- (3) Berciu, M.; Rappoport, T. G.; Janko, B. Manipulating spin and charge in magnetic semiconductors using superconducting vortices. *Nature* **2005**, *435* (7038), 71–75.
- (4) Wang, D. F.; Kong, L. Y.; Fan, P.; Chen, H.; Zhu, S. Y.; Liu, W. Y.; Cao, L.; Sun, Y. J.; Du, S. X.; Schneeloch, J.; Zhong, R. D.; Gu, G. D.; Fu, L.; Ding, H.; Gao, H. J. Evidence for Majorana bound states in an iron-based superconductor. *Science* **2018**, *362* (6412), 333–335.
- (5) Liu, Q.; Chen, C.; Zhang, T.; Peng, R.; Yan, Y.-J.; Wen, C.-H.-P.; Lou, X.; Huang, Y.-L.; Tian, J.-P.; Dong, X.-L.; Wang, G.-W.; Bao, W.-C.; Wang, Q.-H.; Yin, Z.-P.; Zhao, Z.-X.; Feng, D.-L. Robust and clean Majorana zero mode in the vortex core of high-temperature superconductor (Li_{0.84}Fe_{0.16})OHFeSe. *Phys. Rev. X* **2018**, *8* (4), 041056.
- (6) Liu, W.; Cao, L.; Zhu, S.; Kong, L.; Wang, G.; Papaj, M.; Zhang, P.; Liu, Y.-B.; Chen, H.; Li, G.; Yang, F.; Kondo, T.; Du, S.; Cao, G.-H.; Shin, S.; Fu, L.; Yin, Z.; Gao, H.-J.; Ding, H. A new Majorana platform in an Fe-As bilayer superconductor. *Nat. Commun.* **2020**, *11* (1), 5688.
- (7) Kong, L.; Cao, L.; Zhu, S.; Papaj, M.; Dai, G.; Li, G.; Fan, P.; Liu, W.; Yang, F.; Wang, X.; Du, S.; Jin, C.; Fu, L.; Gao, H.-J.; Ding, H. Majorana zero modes in impurity-assisted vortex of LiFeAs superconductor. *Nat. Commun.* **2021**, *12* (1), 4146.
- (8) Li, M.; Li, G.; Cao, L.; Zhou, X.; Wang, X.; Jin, C.; Chiu, C. K.; Pennycook, S. J.; Wang, Z.; Gao, H. J. Ordered and tunable Majorana-zero-mode lattice in naturally strained LiFeAs. *Nature* **2022**, *606* (7916), 890–895.
- (9) Kong, L.; Zhu, S.; Papaj, M.; Chen, H.; Cao, L.; Isobe, H.; Xing, Y.; Liu, W.; Wang, D.; Fan, P.; Sun, Y.; Du, S.; Schneeloch, J.; Zhong, R.; Gu, G.; Fu, L.; Gao, H.-J.; Ding, H. Half-integer level shift of vortex bound states in an iron-based superconductor. *Nat. Phys.* **2019**, *15* (11), 1181–1187.
- (10) Zhu, S. Y.; Kong, L. Y.; Cao, L.; Chen, H.; Papaj, M.; Du, S. X.; Xing, Y. Q.; Liu, W. Y.; Wang, D. F.; Shen, C. M.; Yang, F. Z.; Schneeloch, J.; Zhong, R. D.; Gu, G. D.; Fu, L.; Zhang, Y. Y.; Ding, H.; Gao, H. J. Nearly quantized conductance plateau of vortex zero mode in an iron-based superconductor. *Science* **2020**, *367* (6474), 189–192.
- (11) Machida, T.; Sun, Y.; Pyon, S.; Takeda, S.; Kohsaka, Y.; Hanaguri, T.; Sasagawa, T.; Tamegai, T. Zero-energy vortex bound state in the superconducting topological surface state of Fe(Se,Te). *Nat. Mater.* **2019**, *18* (8), 811–815.
- (12) Fan, P.; Yang, F.; Qian, G.; Chen, H.; Zhang, Y.-Y.; Li, G.; Huang, Z.; Xing, Y.; Kong, L.; Liu, W.; Jiang, K.; Shen, C.; Du, S.; Schneeloch, J.; Zhong, R.; Gu, G.; Wang, Z.; Ding, H.; Gao, H.-J. Observation of magnetic adatom-induced Majorana vortex and its hybridization with field-induced Majorana vortex in an iron-based superconductor. *Nat. Commun.* **2021**, *12* (1), 1348.
- (13) Kitaev, A. Y. Fault-tolerant quantum computation by anyons. *Ann. Phys.* **2003**, *303*, 2–30.
- (14) Nayak, C.; Simon, S. H.; Stern, A.; Freedman, M.; Das Sarma, S. Non-Abelian anyons and topological quantum computation. *Rev. Mod. Phys.* **2008**, *80* (3), 1083–1159.
- (15) Straver, E. W. J.; Hoffman, J. E.; Auslaender, O. M.; Rugar, D.; Moler, K. A. Controlled manipulation of individual vortices in a superconductor. *Appl. Phys. Lett.* **2008**, *93* (17), 172514.
- (16) Auslaender, O. M.; Luan, L.; Straver, E. W. J.; Hoffman, J. E.; Koshnick, N. C.; Zeldov, E.; Bonn, D. A.; Liang, R.; Hardy, W. N.; Moler, K. A. Mechanics of individual isolated vortices in a cuprate superconductor. *Nat. Phys.* **2009**, *5* (1), 35–39.
- (17) Gardner, B. W.; Wynn, J. C.; Bonn, D. A.; Liang, R.; Hardy, W. N.; Kirtley, J. R.; Kogan, V. G.; Moler, K. A. Manipulation of single vortices in YBa₂Cu₃O_{6.354} with a locally applied magnetic field. *Appl. Phys. Lett.* **2002**, *80* (6), 1010–1012.
- (18) Kremen, A.; Wissberg, S.; Haham, N.; Persky, E.; Frenkel, Y.; Kalisky, B. Mechanical control of individual superconducting vortices. *Nano Lett.* **2016**, *16* (3), 1626–30.
- (19) Kalisky, B.; Kirtley, J. R.; Analytis, J. G.; Chu, J. H.; Fisher, I. R.; Moler, K. A. Behavior of vortices near twin boundaries in underdoped Ba(Fe_{1-x}Co_x)₂As₂. *Phys. Rev. B* **2011**, *83* (6), 064511.
- (20) Marchiori, E.; Ceccarelli, L.; Rossi, N.; Lorenzelli, L.; Degen, C. L.; Poggio, M. Nanoscale magnetic field imaging for 2D materials. *Nat. Rev. Phys.* **2022**, *4* (1), 49–60.
- (21) Veshchunov, I. S.; Magrini, W.; Mironov, S. V.; Godin, A. G.; Trebbia, J. B.; Buzdin, A. I.; Tamarat, P.; Lounis, B. Optical manipulation of single flux quanta. *Nat. Commun.* **2016**, *7*, 12801.
- (22) Ge, J. Y.; Gladilin, V. N.; Tempere, J.; Xue, C.; Devreese, J. T.; Van de Vondel, J.; Zhou, Y.; Moshchalkov, V. V. Nanoscale assembly of superconducting vortices with scanning tunnelling microscope tip. *Nat. Commun.* **2016**, *7*, 13880.
- (23) Olson Reichhardt, C. J.; Hastings, M. B. Do vortices entangle? *Phys. Rev. Lett.* **2004**, *92* (15), 157002.
- (24) Zheng, F.; Thi, Q. H.; Wong, L. W.; Deng, Q.; Ly, T. H.; Zhao, J. Critical stable length in wrinkles of two-dimensional materials. *ACS Nano* **2020**, *14* (2), 2137–2144.
- (25) Lim, H.; Jung, J.; Ruoff, R. S.; Kim, Y. Structurally driven one-dimensional electron confinement in sub-5-nm graphene nano-wrinkles. *Nat. Commun.* **2015**, *6*, 8601.

- (26) Liu, L.; Xiao, W.; Wang, D.; Yang, K.; Tao, L.; Gao, H.-J. Edge states of graphene wrinkles in single-layer graphene grown on Ni(111). *Appl. Phys. Lett.* **2016**, *109* (14), 143103.
- (27) Thi, Q. H.; Wong, L. W.; Liu, H.; Lee, C. S.; Zhao, J.; Ly, T. H. Spontaneously ordered hierarchical two-dimensional wrinkle patterns in two-dimensional materials. *Nano Lett.* **2020**, *20* (11), 8420–8425.
- (28) Wang, H.; Li, Y.; Li, Y.; Liu, Y.; Lin, D.; Zhu, C.; Chen, G.; Yang, A.; Yan, K.; Chen, H.; Zhu, Y.; Li, J.; Xie, J.; Xu, J.; Zhang, Z.; Vila, R.; Pei, A.; Wang, K.; Cui, Y. Wrinkled graphene cages as hosts for high-capacity Li metal anodes shown by cryogenic electron microscopy. *Nano Lett.* **2019**, *19* (2), 1326–1335.
- (29) Zhang, Y.; Heiranian, M.; Janicek, B.; Budrikis, Z.; Zapperi, S.; Huang, P. Y.; Johnson, H. T.; Aluru, N. R.; Lyding, J. W.; Mason, N. Strain modulation of graphene by nanoscale substrate curvatures: a molecular view. *Nano Lett.* **2018**, *18* (3), 2098–2104.
- (30) Zhang, R.; Lai, Y.; Chen, W.; Teng, C.; Sun, Y.; Yang, L.; Wang, J.; Liu, B.; Cheng, H. M. Carrier trapping in wrinkled 2D monolayer MoS₂ for ultrathin memory. *ACS Nano* **2022**, *16*, 6309–6316.
- (31) Wang, J.; Han, M.; Wang, Q.; Ji, Y.; Zhang, X.; Shi, R.; Wu, Z.; Zhang, L.; Amini, A.; Guo, L.; Wang, N.; Lin, J.; Cheng, C. Strained epitaxy of monolayer transition metal dichalcogenides for wrinkle arrays. *ACS Nano* **2021**, *15* (4), 6633–6644.
- (32) Wan, J.; Hao, Y.; Shi, Y.; Song, Y. X.; Yan, H. J.; Zheng, J.; Wen, R.; Wan, L. J. Ultra-thin solid electrolyte interphase evolution and wrinkling processes in molybdenum disulfide-based lithium-ion batteries. *Nat. Commun.* **2019**, *10* (1), 3265.
- (33) Cho, C.; Wong, J.; Taqieddin, A.; Biswas, S.; Aluru, N. R.; Nam, S.; Atwater, H. A. Highly strain-tunable interlayer excitons in MoS₂/WSe₂ heterobilayers. *Nano Lett.* **2021**, *21* (9), 3956–3964.
- (34) Iff, O.; Tedeschi, D.; Martin-Sanchez, J.; Moczala-Dusanowska, M.; Tongay, S.; Yumigeta, K.; Taboada-Gutierrez, J.; Savaresi, M.; Rastelli, A.; Alonso-Gonzalez, P.; Hofling, S.; Trotta, R.; Schneider, C. Strain-tunable single photon sources in WSe₂ monolayers. *Nano Lett.* **2019**, *19* (10), 6931–6936.
- (35) Rhuy, D.; Lee, Y.; Kim, J. Y.; Kim, C.; Kwon, Y.; Preston, D. J.; Kim, I. S.; Odom, T. W.; Kang, K.; Lee, D.; Lee, W. K. Ultraefficient electrocatalytic hydrogen evolution from strain-engineered, multilayer MoS₂. *Nano Lett.* **2022**, *22* (14), 5742–5750.
- (36) Yang, S.; Wang, C.; Sahin, H.; Chen, H.; Li, Y.; Li, S. S.; Suslu, A.; Peeters, F. M.; Liu, Q.; Li, J.; Tongay, S. Tuning the optical, magnetic, and electrical properties of ReSe₂ by nanoscale strain engineering. *Nano Lett.* **2015**, *15* (3), 1660–1666.
- (37) Cao, L.; Liu, W.; Li, G.; Dai, G.; Zheng, Q.; Wang, Y.; Jiang, K.; Zhu, S.; Huang, L.; Kong, L.; Yang, F.; Wang, X.; Zhou, W.; Lin, X.; Hu, J.; Jin, C.; Ding, H.; Gao, H. J. Two distinct superconducting states controlled by orientations of local wrinkles in LiFeAs. *Nat. Commun.* **2021**, *12* (1), 6312.
- (38) Li, X. S.; Cai, W. W.; An, J. H.; Kim, S.; Nah, J.; Yang, D. X.; Piner, R.; Velamakanni, A.; Jung, I.; Tutuc, E.; Banerjee, S. K.; Colombo, L.; Ruoff, R. S. Large-area synthesis of high-quality and uniform graphene films on copper foils. *Science* **2009**, *324* (5932), 1312–1314.
- (39) Liang, R.; Bonn, D. A.; Hardy, W. N. Evaluation of CuO₂ plane hole doping in YBa₂Cu₃O_{6+x} single crystals. *Phys. Rev. B* **2006**, *73* (18), 180505.
- (40) Llordes, A.; Palau, A.; Gazquez, J.; Coll, M.; Vlad, R.; Pomar, A.; Arbiol, J.; Guzman, R.; Ye, S.; Rouco, V.; Sandiumenge, F.; Ricart, S.; Puig, T.; Varela, M.; Chateigner, D.; Vanacken, J.; Gutierrez, J.; Moshchalkov, V.; Deutscher, G.; Magen, C.; Obradors, X. Nanoscale strain-induced pair suppression as a vortex-pinning mechanism in high-temperature superconductors. *Nat. Mater.* **2012**, *11* (4), 329–336.
- (41) Massee, F.; Sprau, P. O.; Wang, Y. L.; Davis, J. C. S.; Ghigo, G.; Gu, G. D.; Kwok, W. K. Imaging atomic-scale effects of high-energy ion irradiation on superconductivity and vortex pinning in Fe(Se, Te). *Sci. Adv.* **2015**, *1* (4), e1500033.
- (42) Xing, L. Y.; Miao, H.; Wang, X. C.; Ma, J.; Liu, Q. Q.; Deng, Z.; Ding, H.; Jin, C. Q. The anomaly Cu doping effects on LiFeAs superconductors. *J. Phys.: Condens. Matter* **2014**, *26* (43), 435703.